DIGITAL ACCESS TO SCHOLARSHIP AT HARVARD
DASH.HARVARD.EDU

HARVARD LIBRARY
Office for Scholarly Communication

A co-clinical approach identifies mechanisms and potential therapies for androgen deprivation resistance in prostate cancer

Citation

Lunardi, A., U. Ala, M. T. Epping, L. Salmena, J. G. Clohessy, K. A. Webster, G. Wang, et al. 2013. "A co-clinical approach identifies mechanisms and potential therapies for androgen deprivation resistance in prostate cancer." Nature genetics 45 (7): 747-755. doi:10.1038/ng.2650. http://dx.doi.org/10.1038/ng.2650.

Published Version

doi:10.1038/ng.2650

Permanent link

http://nrs.harvard.edu/urn-3:HUL.InstRepos:11879681

Terms of Use

This article was downloaded from Harvard University's DASH repository, and is made available under the terms and conditions applicable to Other Posted Material, as set forth at http://nrs.harvard.edu/urn-3:HUL.InstRepos:dash.current.terms-of-use#LAA

Share Your Story

The Harvard community has made this article openly available.
Please share how this access benefits you. Submit a story .

Accessibility

NIH Public Access
Author Manuscript
Nat Genet. Author manuscript; available in PMC 2014 January 01.

Published in final edited form as:
Nat Genet. 2013 July ; 45(7): 747–755. doi:10.1038/ng.2650.

A co-clinical approach identifies mechanisms and potential therapies for androgen deprivation resistance in prostate cancer

Andrea Lunardi[1], **Ugo Ala**[1,2], **Mirjam T. Epping**[1], **Leonardo Salmena**[1,3,4], **John G. Clohessy**[1], **Kaitlyn A. Webster**[1], **Guocan Wang**[1,3,4,5], **Roberta Mazzucchelli**[6], **Maristella Bianconi**[7], **Edward C. Stack**[8,9,10], **Rosina Lis**[8,9], **Akash Patnaik**[11], **Lewis C. Cantley**[12,13], **Glenn Bubley**[11], **Carlos Cordon-Cardo**[14], **William L. Gerald**[4], **Rodolfo Montironi**[6], **Sabina Signoretti**[9,10], **Massimo Loda**[8,9,15], **Caterina Nardella**[1,3,4,16], and **Pier Paolo Pandolfi**[1,3,4]

[1]Cancer Genetics Program, Beth Israel Deaconess Cancer Center, Department of Medicine and Pathology, Beth Israel Deaconess Medical Center, Harvard Medical School, Boston MA 02115, USA.

[2]Department of Genetics, Biology and Biochemistry, Molecular Biotechnology Center, University of Turin, Turin, Italy.

[3]Cancer Biology and Genetics Program, Sloan-Kettering Institute, Human Oncology and Pathogenesis Program, Memorial Sloan-Kettering Cancer Center, 1275 York Avenue, New York, New York 10021, USA.

[4]Department of Pathology, Human Oncology and Pathogenesis Program, Memorial Sloan-Kettering Cancer Center, 1275 York Avenue, New York, New York 10021, USA.

[5]BCMB Program, Weill Graduate School of Medical Sciences, Cornell University, New York, New York 10021.

[6]Institute of Pathological Anatomy and Histopathology, Polytechnic University of the Marche Region (Ancona), United Hospitals, Ancona, Italy.

[7]Clinic of Oncology, Postgraduate School in Medical Oncology, Polytechnic University of the Marche Region (Ancona), United Hospitals, Ancona, Italy.

[8]Center for Molecular Oncologic Pathology, Dana-Farber Cancer Institute, Boston, MA 02115, USA.

[9]Department of Medical Oncology, Dana-Farber Cancer Institute, Harvard Medical School, Boston, MA 02115, USA.

[10]Department of Pathology, Brigham and Women's Hospital, Harvard Medical School, Boston, MA 02115, USA.

[11]Division of Hematology/Oncology, Beth Israel Deaconess Medical Center, Harvard Medical School, Boston, MA 02115, USA.

[12]Department of Systems Biology, Harvard Medical School, Boston, MA 02115, USA.

Correspondence to: ppandolf@bidmc.harvard.edu.

AUTHOR CONTRIBUTIONS

A.L., C.N., and P.P.P. designed, realized and analyzed the experiments. U.A., W.L.G., R.M., M.B, E.C.S., R.L., A.P., L.C.W., G.B., C.C., W.L.G., and R.M., conducted the human genetic and molecular analysis. K.A.W. performed the H&E and IHC on mouse prostate samples. M.T.E, L.S., J.G.C., and G.W., helped with the experiments. M.L. and S.S. reviewed all mouse pathology. A.L., C.N., and P.P.P. wrote the manuscript.

COMPETING INTERESTS STATEMENT

The authors declare no competing financial interests.

NIH-PA Author Manuscript
NIH-PA Author Manuscript
NIH-PA Author Manuscript

NIH-PA Author Manuscript

NIH-PA Author Manuscript

NIH-PA Author Manuscript

[13]Division of Signal Transduction, Beth Israel Deaconess Medical Center, Boston, MA 02115, USA.

[14]Department of Genetics and Genomic Sciences, The Mount Sinai School of Medicine, New York, NY 10029, USA.

[15]Broad Institute of Harvard and Massachusetts Institute of Technology, Cambridge, MA 02215, USA.

[16]Preclinical Murine Pharmacogenetics Facility, Beth Israel Deaconess Medical Center, Harvard Medical School, Boston, MA 02115, USA.

Abstract

Here we report an integrated analysis that leverages data from treatment of genetic mouse models of prostate cancer along with clinical data from patients to elucidate new mechanisms of castration resistance. We show that castration counteracts tumor progression in a *Pten*-loss driven mouse model of prostate cancer through the induction of apoptosis and proliferation block. Conversely, this response is bypassed upon deletion of either *Trp53 or Lrf* together with *Pten*, leading to the development of castration resistant prostate cancer (CRPC). Mechanistically, the integrated acquisition of data from mouse models and patients identifies the expression patterns of XAF1-XIAP/SRD5A1 as a predictive and actionable signature for CRPC. Importantly, we show that combined inhibition of XIAP, SRD5A1, and AR pathways overcomes castration resistance. Thus, our co-clinical approach facilitates stratification of patients and the development of tailored and innovative therapeutic treatments.

We conceived the co-clinical platform as an innovative approach to improve the design, speed and outcomes of rational and personalized clinical treatments[1]. The power of this approach lies in harnessing data gained from pre-clinical studies performed in several genetic mouse models and combining it with the concurrent investigation of therapies, either conventional or experimental, in human patients.

One goal of this approach is to expedite the identification of key genetic and molecular determinants that dictate resistance to a specific therapy in order to facilitate the stratification of human candidates for enrollment in treatment with different therapies, optimize combination treatments and accelerate new drug approval.

In this study we have implemented this paradigm in an investigation of androgen deprivation therapy (ADT), which is a widely-prescribed standard-of-care therapy for prostate cancer. Although almost invariably effective in the short term, ADT is consistently followed by the development of castration resistant prostate cancer (CRPC) in the majority of patients[2]. Given the diverse genetic alterations reported to drive prostate cancer initiation and progression, we hypothesized that these same genetic alterations also govern the tumor response to ADT, and may be utilized to develop novel combinational treatments.

Testing this hypothesis with the co-clinical approach led to the discovery of new pathways underlying ADT resistance, as well as new potential modalities for overcoming this serious therapeutic hurdle.

RESULTS

Prostate cancer genetic dictates androgen deprivation response

PTEN, LRF, and *TP53* loss or mutation has been associated with prostate cancer progression in human and mouse models (**Supplementary Table 1**)[4-12]. We therefore enrolled prostate

NIH-PA Author Manuscript

NIH-PA Author Manuscript

NIH-PA Author Manuscript

conditional *Pten* null mice (*Pten*$^{flox/flox}$*;Probasin-Cre*), *Pten* and *Lrf* double null mice (*Pten*$^{flox/flox}$*;Lrf*$^{flox/flox}$*;Probasin-Cre*), and *Pten* and *p53* double null mice (*Pten*$^{flox/flox}$*;p53*$^{flox/flox}$*;Probasin-Cre*) to test the hypothesis that advanced prostate cancer with distinct genetic makeups respond differentially to ADT. For each genetically-distinct tumor type, we generated cohorts of 15 mutant mice that were castrated at the age at which they had developed prostate cancer (high grade-prostatic epithelial neoplasia (HG-PIN) characterized by focal invasive carcinoma) as previously reported[4,5,13]. Age-matched non-castrated cohorts were used as controls. All cohorts were monitored for 3 months post-castration.

Groups of 5 mice from each cohort (castrated and non-castrated) were sacrificed at 1, 2 and 3 months post-castration for histopathological analysis (see **Fig. 1a** for timeline of the analysis). Mice from the 3-month post-castration group were also imaged by magnetic resonance imaging (MRI) for tumor volume assessment on a monthly schedule (**Fig. 1a**).

Histopathological analysis of *Pten*$^{flox/flox}$*;Probasin-Cre* mice at 1 and 2 months post-castration identified the presence of a significant amount of normal epithelium in castrated mice, indicative of a clear response to castration, when compared to the levels of normal epithelium in the non-castrated control group [1 month: PI 0 = 25% vs 0 < 5%, ($p < 0.01$) in **Supplementary Fig. 1a** left panel and 2 months: PI 0 = 40% vs. 0 < 5%, ($p < 0.01$) **Fig. 1b** left panels and **Supplementary Fig. 1a**]. Importantly, and in agreement with a previous report[14], examination of the DLP from castrated *Pten*$^{flox/flox}$*;Probasin-Cre* mice at 3 months post-castration demonstrated a strong reduction of normal epithelium, indicating onset of acquired resistance to ADT (**Fig. 1c** left panel and **Supplementary Fig. 1a**). In sharp contrast to this finding, we did not observe any response in DLP from either castrated *Pten*$^{flox/flox}$*;Lrf*$^{flox/flox}$*;Probasin-Cre* (**Fig. 1b-c** center panels and **Supplementary Fig. 1a**) or *Pten*$^{flox/flox}$*;p53*$^{flox/flox}$*;Probasin-Cre* mutants (**Fig. 1b-c** right panels and **Supplementary Fig. 1a**). These results indicate that loss of either *p53* or *Lrf* in a *Pten*-null genetic context confers a *de novo* resistance to androgen deprivation in the DLP tumors.

Interestingly, and in line with recent publications[15], examination of the ventral lobe of the mouse prostate (VP) from castrated *Pten*$^{flox/flox}$*;Probasin-Cre* mice identified, an intrinsic propensity of the tumors derived from this lobe to be resistant to ADT (PI 0 = 0%; **Supplementary Fig. 1b**).

The anterior lobe of the mouse prostate (AP) of Pten$^{flox/flox}$;Probasin-Cre, Pten$^{flox/flox}$;Lrf$^{flox/flox}$;Probasin-Cre, Pten$^{flox/flox}$;p53$^{flox/flox}$;Probasin-Cre mice are characterized by a marked cystic dilation of prostate ducts[5], a feature preventing accurate pathological evaluation of the extent and severity of tumor lesions. Therefore, to assess ADT responses in this lobe, we quantitated the tumor volume of AP lesions by MRI (**Fig. 1d**). In line with the results described for the DLP above, we observed that castration of *Pten*$^{flox/flox}$*;Probasin-Cre* led to reduced tumor volumes (**Fig. 1d** upper panels), while no regression was observed in castrated *Pten*$^{flox/flox}$*;Lrf*$^{flox/flox}$*;Probasin-Cre* (**Fig. 1d** middle panels) and *Pten*$^{flox/flox}$*;p53*$^{flox/flox}$*;Probasin-Cre* mice (**Fig. 1d** lower panels).

In accordance with the results obtained through physical castration, *Pten*$^{flox/flox}$*;Probasin-Cre* mice displayed sensitivity (as previously described)[16] while *Pten*$^{flox/flox}$*;Lrf*$^{flox/flox}$*;Probasin-Cre* and *Pten*$^{flox/flox}$*;p53*$^{flox/flox}$*;Probasin-Cre* mice displayed resistance to chemical castration (bicalutamide), thereby validating that resistance to ADT is tumor-intrinsic and not dependent on the specific treatment (**Supplementary Fig. 1c-f**).

NIH-PA Author Manuscript

NIH-PA Author Manuscript

NIH-PA Author Manuscript

Together, these data demonstrate that *Pten*-null prostate cancer is initially sensitive to androgen deprivation, yet invariably acquires castration-resistance. In contrast, our analysis clearly demonstrates that both *Pten;Lrf* and *Pten;p53* double null prostate cancers display complete resistance to castration.

Genetic determinants of ADT response in human patients

We next determined whether the differential response to castration we observed in the different mouse models would allow us to predict responses to ADT in human prostate cancer (**Fig. 2a**). To this end, we constructed a tissue microarray (TMA) designed to interrogate ADT response biomarkers by immunohistochemistry (IHC). The TMA included 84 biopsied specimens from prostatectomized human primary prostate cancer (Gleason Score 6/7) that had been treated with neo-adjuvant ADT and showed variable response to the treatment, as measured by the ratio in circulating prostate specific antigen (PSA) levels before and after ADT, proliferation rate and percentage of cells with nuclear AR localization (Fig. 2b, Supplementary Fig. 2a-c, Supplementary Table 2 and **Supplementary Note**). We also performed an additional analysis to validate our stratification criteria. It has been previously reported that levels of 10 ng/ml of PSA at diagnosis are frequently predictive of worse prognosis when compared with patients with levels below 10 ng/ml [reviewed in Ref.[17,18]]. 31 of our patients (out of 84) had a PSA value higher than 10 ng/ml before treatment with ADT in neo-adjuvant setting (**Supplementary Fig. 2c**). After 3 months on ADT, patients have now been classified as either good (16 patients) or poor responders (15 patients) based on the ratio of PSA levels after and before treatment (**Supplementary Fig. 2c**). Importantly, all the patients that retained levels of PSA > 10 ng/ml post-ADT belonged to the category of poor responder (11 out of 15) and none was found among the 16 good responders (p=1.612E-05; **Supplementary Fig. 2c**). Finally, we obtained and analyzed the follow-up information of 36 of the 84 patients originally enrolled in this study. Notably, only 2 out of 23 patients classified as “Good Responders” have developed resistance to ADT, while a consistent 6 out of 13 belong to the category of the “Poor Responders” (p=0.01; **Supplementary Fig. 2d**). These data further suggest the notion that the category that we have identified as poor responder represents the group of patients most likely to develop tumor recurrence and castration-resistant distant metastasis [reviewed in Ref.[17,18]].

As mentioned, *TP53* loss or mutation has been associated with tumor progression in a subset of human patients (**Supplementary Table 1**)[6-11]. Taking into account that p53 loss cannot be evaluated by IHC, as the protein levels are usually extremely low, on our TMA we could only assess mutational events, which would result in p53 overexpression. Mutation in p53 has been reported to correlate with progression to higher Gleason Scores (4 + 3 or 4 + 4) and CRPC[6], while the patients in our TMA had lower Gleason Scores (mainly 3 + 3 and 3 + 4 as detailed in the **Supplementary Table 2**). In agreement with these findings, in these earlier prostate cancer lesions from our cohort we could not identify any sample with a homogeneously elevated p53 immunohistochemical staining. We therefore interrogated a pre-existing array-based comparative genomic hybridization (aCGH) database made up of 37 human prostate cancer metastases (28 out of 37 were castration resistant)[11]. 43% of these castration resistant metastatic patients (12 of 28) presented heterozygous loss and 7% homozygous loss (2 out of 28) of p53, thereby confirming the relevance of loss in this tumor suppressor gene in CRPC.

We next focused our attention on PTEN and LRF and performed IHC on our low-Gleason TMAs (**Fig. 2c-d**). In this analysis, we observed no difference in the mean PTEN loss in those patients who responded poorly or favorably to ADT (**Fig. 2c**). In contrast, patient tumors harboring a significantly larger mean number of LRF-null cells stratified as poor responders to ADT (**Fig. 2d**). Additionally, the number of patients that displayed both

NIH-PA Author Manuscript

NIH-PA Author Manuscript

NIH-PA Author Manuscript

PTEN- and LRF-protein loss was 15 out of 84 total samples, 4 in the category of good responders (4/48 patients, 8.7%) and 11 in the category of poor responders (11/36 patients, 30.5%) (**Fig. 2e**, p=0.0132), suggesting that concomitant loss of *PTEN* and *LRF* stratifies for poor responsiveness to castration.

In order to mirror in humans the data obtained in genetic mouse models, we sought to assess in prostate cancer patients whether concomitant genetic loss of *LRF* with *PTEN* may be a stronger indicator of CRPC development than loss of *PTEN* only. To this end, we interrogated again the aCGH database made up of 37 human prostate cancer metastases (28 out of 37 were castration resistant)[11]. We identified 336 genes undergoing genetic losses solely in castration-resistant specimens characterized by concomitant loss of *PTEN* in at least 80% of cases (**Supplementary Fig. 2e** and **Supplementary Table 3**). Intriguingly, 110 of these genes were located on the telomeric p arm of chromosome 19 (**Supplementary Fig. 2e**) including *LRF* gene (*Zbtb7a*) (**Fig. 2f**). This suggests that in humans, as predicted by our mouse study, there is a functional association between loss of *PTEN* and genetic deletion of *LRF* for CRPC development (**Fig. 2g and Supplementary Fig. 2f**).

The relevance of LRF loss in CRPC was further confirmed by the analysis of two other large pre-existing aCGH datasets made up of 58 and 50 human castration resistant metastatic prostate cancer samples[19,20]. LRF was found to be genetically lost in 26% of cases (15 out of 58), and in 33% of cases (15 out of 50) respectively[19,20]. In particular, 10 castration resistant metastatic specimens out of 15 (67%) in the first dataset[19] and 8 out of 15 (53%) in the second dataset[20] showed specific deletion of the telomeric p arm of chromosome 19 which contains the *LRF* gene (*Zbtb7a*) (**Fig. 2h**, and **Supplementary Fig. 2g**). Of note, in the dataset recently published by Grasso and colleagues[20], 2 out of 3 described castration resistant bone marrow metastases show deletion of the telomeric p arm of chromosome 19 (WA48, and WA51), while the remaining one (WA23) is characterized by a somatic missense mutation (K60R) in the BTB/POZ domain of LRF, a fundamental region for its transcriptional repressive activity[21].

Finally, a similar result was also obtained by the analysis of the expression profile data set from Tomlins et al.[22], where we observed a significant reduction in *LRF* expression in castration resistant metastases (20) from several organs (**Fig. 2i**), thereby further corroborating a role for *LRF* loss in resistance to ADT.

Together, these data show that prostate cancers characterized by distinct genetic background differentially respond to ADT in mice as well as human patients, and that *LRF* represents an unexpected player in the response of prostate cancer to androgen deprivation.

Biological responses to androgen deprivation

Castration typically results in a major decrease in prostatic mass, with the key molecular hallmarks including decreased proliferation and increased apoptosis[23]. Accordingly, we examined whether the absence of androgen differentially affects the proliferative index of these tumor types. To this end, we performed IHC on the VP, DLP, and AP of castrated mice utilizing the cellular proliferation marker Ki67. In $Pten^{flox/flox}$;*Probasin-Cre* mice we observed at one month post-castration a significant reduction in the overall proliferative index (**Fig. 3a and 3b** for quantifications, left panels). In contrast, we observed no difference in the proliferative index in any prostate lobes from either $Pten^{flox/flox}$;$Lrf^{flox/flox}$;*Probasin-Cre* mice (**Fig. 3a and 3b** for quantifications, center panels), or $Pten^{flox/flox}$;$p53^{flox/flox}$;*Probasin-Cre* (**Fig. 3a and 3b** for quantifications, right panels) at one month post-castration compared to non-castrated controls. These findings suggest that *Lrf* or *p53* deletion in *Pten*-null prostate epithelium confers an ability to

NIH-PA Author Manuscript

NIH-PA Author Manuscript

NIH-PA Author Manuscript

proliferate in conditions of androgen depletion. Notably, no difference in Ki67 staining was observed in the VP of the same mice (**Supplementary Fig. 3a**).

We next measured the induction of apoptosis in the prostatic epithelium of castrated Pten$^{flox/flox}$;Probasin-Cre, Pten$^{flox/flox}$;Lrf$^{flox/flox}$;Probasin-Cre, and *Pten$^{flox/flox}$;p53$^{flox/flox}$;Probasin-Cre* mice. The induction of an early apoptotic response was observed in all lobes of the prostate and in all genotypes, as analyzed by measuring elevation of caspase-3 cleavage (**Fig. 3c**). In contrast, Parp cleavage and pyknotic nuclei (**Supplementary Fig. 3b**), feature of terminal apoptosis, were observed in all prostate lobes of castrated *Pten$^{flox/flox}$;Probasin-Cre* mice (**Fig. 3c**), but were completely absent in all lobes of *Pten$^{flox/flox}$;Lrf$^{flox/flox}$;Probasin-Cre,* and *Pten$^{flox/flox}$;p53$^{flox/flox}$;Probasin-Cre* castrated mice, indicating apoptotic inhibition in these tumors.

We next investigated the effects of androgen withdrawal on androgen receptor (AR) localization in our different prostate cancer genotypes. AR was predominantly translocated to the cytoplasm in all genotypes shortly after castration, as expected in the absence of androgen[24] (**Fig. 3d** for DLP and AP, **Supplementary Fig. 3c** for VP). However, quantitative IHC analysis of prostates from castrated *Pten$^{flox/flox}$;Lrf$^{flox/flox}$;Probasin-Cre,* and *Pten$^{flox/flox}$;p53$^{flox/flox}$;Probasin-Cre* mice identified a modest but significantly greater number of cells with nuclear AR compared to the prostates of castrated *Pten$^{flox/flox}$;Probasin-Cre* mice (**Fig. 3e** and relevant quantification), suggesting that cells switch to or harbor pre-existing alternative pathways of AR activation in *Pten;Lrf* or *Pten;p53* double null CRPC (see below).

In summary, these data suggest that *Pten;Lrf* or *Pten;p53* double null tumor prostatic cells, in contrast to *Pten*-null only, posses the ability to sustain androgen-independent proliferation, while escaping the engagement of an apoptotic response.

XAF1 and SRD5A1 are key biomarkers for ADT response in mouse and human

Next we sought to identify the molecular mechanisms underlying the differential sensitivity displayed by Pten$^{flox/flox}$;Probasin-Cre vs. Pten$^{flox/flox}$;Lrf$^{flox/flox}$;Probasin-Cre and *Pten$^{flox/flox}$;p53$^{flox/flox}$;Probasin-Cre* double null prostate tumor cells when challenged by androgen deprivation. For this purpose, we interrogated microarray gene expression profiles from mouse prostate specimens[4]. Strikingly, we observed a significant down-regulation (p=1.07E-12) of X-linked inhibitor of apoptosis protein-associated factor-1 (*Xaf1*; **Fig. 4a**) in *Pten$^{flox/flox}$;Lrf$^{flox/flox}$;Probasin-Cre* mice compared to *Pten$^{flox/flox}$;Probasin-Cre*. XAF1 was first identified as a protein that binds and opposes the anti-caspase activity of X-linked inhibitor of apoptosis (XIAP), thereby promoting apoptosis[25]. A growing body of evidence has also demonstrated strong involvement of the XAF1-XIAP pathway in cell cycle regulation through yet unknown mechanisms[26-32]. The down-regulation of Xaf1 was confirmed by qRT-PCR, IHC and Western blot in specimens from *Pten$^{flox/flox}$;Lrf$^{flox/flox}$;Probasin-Cre* mice (**Fig. 4b-d**). Since XAF1 has been recently reported to be a p53-responsive gene[33], we assessed Xaf1 levels in *Pten$^{flox/flox}$;p53$^{flox/flox}$;Probasin-Cre* mice. As expected, *Xaf1* was significantly down-regulated in *Pten$^{flox/flox}$;p53$^{flox/flox}$;Probasin-Cre* prostates as measured by qRT-PCR, IHC and Western blot (**Fig. 4b-d**). Interestingly, IHC of Xaf1 in DLP from castrated *Pten$^{flox/flox}$;Probasin-Cre* mice analyzed 90 days post-castration showed reduced levels of staining-positive cells compared to ones analyzed 30 days post-castration, supporting the concept of Xaf1 as a good biomarker for castration resistance (**Supplementary Fig. 4a**).

Further interrogation of expression profiles of *Pten$^{flox/flox}$;Lrf$^{flox/flox}$;Probasin-Cre* murine prostates identified a significant up-regulation of *3-oxo-5-alpha-steroid 4-dehydrogenase 1* (*Srd5a1*) gene compared to *Pten$^{flox/flox}$;Probasin-Cre* mice (**Fig. 4a**). Srd5a1 and Srd5a2

NIH-PA Author Manuscript

NIH-PA Author Manuscript

NIH-PA Author Manuscript

enzymes catalyze the conversion of testosterone into dihydrotestosterone (DHT), a more potent and stable form of testosterone, and Srd5a1 is known to be frequently up-regulated in human CRPC[35]. Production of DHT represents an important alternative mechanism that allows activation of AR at castration-levels of androgen[35]. qRT-PCR on the prostates from *Pten*$^{flox/flox}$*;Lrf*$^{flox/flox}$*;Probasin-Cre* and *Pten*$^{flox/flox}$*;p53*$^{flox/flox}$*;Probasin-Cre* mice confirmed *Srd5a1* up-regulation compared to *Pten*$^{flox/flox}$*;Probasin-Cre* prostate cancer (**Fig. 4e**), while no changes in the level of *Srd5a2* transcript were observed (**Supplementary Fig. 5a**). Interestingly, qRT-PCR analysis in DLP from castration resistant *Pten*$^{flox/flox}$*;Probasin-Cre* mice analyzed 90 days post-castration also showed higher levels of Srd5a1 compared to the castration sensitive *Pten*$^{flox/flox}$*;Probasin-Cre* prostates analyzed 30 days post-castration, whereas only a mild increase was observed in the level of Srd5a2 (**Supplementary Fig. 4b**). Notably, while Western blot analysis of AR in DLP from castrated *Pten*$^{flox/flox}$*;Probasin-Cre* mice analyzed 90 days post-castration showed no differences in the levels of the protein compared to ones analyzed 30 days post-castration (**Supplementary Fig. 4a**), IHC analysis showed different localization of AR in the two different contexts. In the castration sensitive setting (30 days after castration) AR, as expected, was mainly localized in the cytoplasm. In contrast, AR was found to be nuclear 90 days post castration in large areas of the *Pten*$^{flox/flox}$*;Probasin-Cre* mutant tumor, as frequently observed in human prostate cancers that have acquired resistance to ADT[34], and Western blot analysis showed higher levels of the AR transcriptional target Probasin (**Supplementary Fig. 4a**).

In order to translate the relevance of biomarkers found in the mouse to the human context, we assessed the status of XAF1 and SRD5A1 pathways in human prostate cancer. For this, we performed IHC with anti-XAF1 on the custom TMA mentioned above (**Fig. 4f**), and quantitated the number of cells that had down-regulation of XAF1 (**Fig 4f**, right panel). In this analysis, we observed that XAF1 protein levels are lower in human prostate cancer and XAF1 staining is significantly lost in those patients that respond poorly to ADT (**Fig. 4f**).

Furthermore, we analyzed the expression of *XAF1/XIAP and SRD5A1* mRNA in several human prostate cancer expression arrays (**Fig. 4g-l**)[11,36-39]. Importantly, we observed that the expression levels of *XAF1* are significantly decreased, in contrast to *XIAP* and *SRD5A1*, which were significantly increased, in the patients with the most aggressive prostate cancer, as characterized by Gleason Score, recurrence and metastasis (**Fig. 4g-l**). This data, combined with the results obtained in an androgen deprivation setting, suggests that down-regulation of XAF1 and up-regulation of SRD5A1 in high Gleason Score prostate cancer and metastasis might be predictive of poor sensitivity to ADT.

XIAP inhibition sensitizes castration resistant prostate cancers to ADT

Our findings suggest a potential therapeutic modality based on the combination of ADT with a XIAP inhibitor for CRPC. Therefore, we treated the AR-mutant/DHT-sensitive LnCaP C4-2 and the AR-null/DHT-insensitive DU145 and PC3 cell lines with the plant-derived XIAP inhibitor embelin[32] and ADT [charcoal/dextran treated steroid-free FBS (SFM)] as single agents and in combination (**Supplementary Fig. 6a-d**). While single treatments with SFM or embelin at a concentration of 5 μM for 4 days did not induce any apoptosis, the combination of embelin and SFM triggered a clear increase in the apoptotic response in LnCaP C4-2 cells, as measured by PARP cleavage (**Supplementary Fig. 6a**). Notably, the combination of embelin with SFM and MDV3100 (an experimental androgen receptor antagonist drug developed for the treatment of castration-resistant prostate cancer currently in Phase III clinical trial) strikingly increased the apoptotic response in LnCaP C4-2 castration resistant cell line (**Supplementary Fig. 6a**). Likewise XIAP silencing induced apoptosis in SFM conditions (**Supplementary Fig. 6b**), confirming the fundamental role of XAF1/XIAP pathway in human CRPC. As expected, the AR-null DU145 and PC3 prostate

NIH-PA Author Manuscript

NIH-PA Author Manuscript

NIH-PA Author Manuscript

cancer cell lines displayed *de novo* resistance to the SFM-plus-embelin combination treatment since SFM (mimicking ADT) is unable to trigger any apoptotic response in these cell lines (**Supplementary Fig. 6c-d**). Conversely, in these cells ionizing radiation (IR) synergizes with embelin by triggering apoptosis[40].

To corroborate our *in vitro* results *in vivo*, we next enrolled our castration-resistant *Pten*$^{flox/flox}$;*Lrf*$^{flox/flox}$;*Probasin-Cre* and *Pten*$^{flox/flox}$;*p53*$^{flox/flox}$;*Probasin-Cre* mouse models in treatment programs with embelin and ADT. Specifically, we treated 4 month-old *Pten*$^{flox/flox}$;*Lrf*$^{flox/flox}$;*Probasin-Cre* and 3 month-old *Pten*$^{flox/flox}$;*p53*$^{flox/flox}$;*Probasin-Cre*mice with bicalutamide (Casodex) or embelin alone and in combination. Remarkably, while both *Pten*$^{flox/flox}$;*Lrf*$^{flox/flox}$;*Probasin-Cre* and *Pten*$^{flox/flox}$;*p53*$^{flox/flox}$;*Probasin-Cre* prostate cancers exhibited resistance to bicalutamide or embelin treatment as single agents (**Supplementary Fig. 7a-b**), all prostate lobes showed a marked tumor regression when treated with bicalutamide in combination with embelin (**Fig. 5a and Supplementary Fig. 7a-b**). Specifically, we found that treatment of*Pten*$^{flox/flox}$;*Lrf*$^{flox/flox}$;*Probasin-Cre* and *Pten*$^{flox/flox}$;*p53*$^{flox/flox}$;*Probasin-Cre* prostate cancers with bicalutamide plus embelin was characterized by a profound reduction in the proliferation rate (**Fig. 5b-e**), which in the case of *Pten*$^{flox/flox}$;*Lrf*$^{flox/flox}$;*Probasin-Cre* prostate cancers was also accompanied by the rescue of the apoptotic response (**Fig. 5f-g** and **Supplementary Fig. 7c-d**).

These findings clearly demonstrate that castration-resistant prostate tumors characterized by the impairment of the XAF1/XIAP pathway become sensitive to ADT when treated with the XIAP inhibitor embelin.

Combination of ADT, embelin and dutasteride for the treatment of CRPC

We hypothesized that management of CRPC could further benefit from the addition of an SRD5A1 inhibitor to the combination therapy with embelin and ADT. Importantly, the SRD5A1 inhibitor dutasteride is currently utilized in clinical trials in combination with ADT for the treatment of advanced prostate cancer (see URLs)[41-43].

At first, therefore, we treated the VCaP, LnCaP and 22RV1 human prostate cell lines with embelin, dutasteride and ADT as single agents and in triple combination. Strikingly, the triple combination of embelin plus dutasteride and SFM induced an even more potent apoptotic response compared to each of the double combinations, embelin plus SFM and dutasteride plus SFM (**Fig. 6a-d and Supplementary 6e-f**).

We next treated castration resistant 4 month-old *Pten*$^{flox/flox}$;*Lrf*$^{flox/flox}$;*Probasin-Cre* and 3 month-old *Pten*$^{flox/flox}$;*p53*$^{flox/flox}$;*Probasin-Cre* mice with ADT in combination with embelin and dutasteride. Both *Pten;Lrf* and *Pten;p53* double-null prostate cancers exhibited a further significant decrease in tumor burden after the triple treatment with bicalutamide, embelin, and dutasteride when compared to the treatment with the dual combination bicalutamide plus embelin (**Fig. 6e**).

These findings clearly demonstrate that castration-resistant prostate tumors characterized by the impairment of the XAF1/XIAP and SRD5A1 pathways are sensitized to ADT when treated with embelin and dutasteride, thereby rendering this triple combination an effective novel therapeutic approach to the treatment of XAF1/XIAP/SRD5A1 genetically stratified CRPC patients.

DISCUSSION

Our data support the hypothesis that the response to ADT is dictated by the genetic make-up of prostate cancer. Our findings argue that genetic mouse models can be extremely valuable

NIH-PA Author Manuscript

NIH-PA Author Manuscript

NIH-PA Author Manuscript

in tailoring the administration of standard-of-care treatments on the basis of genetic and molecular stratification.

We find that *Pten*-loss driven prostate cancer exhibits an overall reduction in tumor volume in response to castration, indicating that this genetic mouse model is initially sensitive to androgen deprivation. Nevertheless, the mice demonstrate a rapid recurrence of prostate cancer at 3 months post-castration. CRPC development in *Pten*-null prostate cancer appears to be accompanied by concomitant down-regulation of Xaf1, up-regulation of Srd5a1, and re-localization of AR in the nucleus (**Supplementary Fig. 4a**).

This model of "acquired" resistance is consistent with the initial response patterns and invariable latent resistance observed in human prostate cancer subjects. Importantly, we have now shown that concomitant *Pten* and either *Lrf* or *p53* deletions abrogate the response of *Pten*-null tumors to ADT.

Lrf- and *p53*-loss associated castration resistant prostate cancers exhibit low levels of Xaf1, a phenomenon which potentially explains the lack of both apoptosis induction and proliferation arrest. The importance of this pathway is further highlighted by the observation that XIAP is highly up-regulated during prostate cancer progression and CRPC both in human[44] and mice (**Supplementary Fig. 5b**). Accordingly, we have shown that the XIAP inhibitor embelin, when combined with ADT, potently suppresses tumor growth *in vitro*, confirming what previously reported[45], and *in vivo* in our castration resistant genetic mouse models.

We also found that *Pten;Lrf* and *Pten;p53* double null CRPCs, as well as *Pten* null CRPC, are characterized by the up-regulation of *Srd5a1*[35], and, importantly, that dutasteride (SRD5A1 inhibitor) further increases prostate tumor response to embelin plus ADT.

We think our integrated mouse and human analysis has identified potential new therapeutic strategies. Patients with prostate cancer characterized by *XAF1-XIAP/SRD5A1* deregulations are likely to quickly develop CRPC, thus ADT in such patients should be combined with embelin and dutasteride (**Supplementary Fig. 7e**).

In sum, our study demonstrates the validity of a cross-species integrated genetic approach to the evaluation of prostate cancer therapies. A particularly powerful aspect of the approach is the combined access it affords to data regarding genetic and molecular differences between tumors whether in human patients or mouse models. Importantly, this study has led to the identification of critical pathways and genetic alterations dictating responses to standard-of-care therapeutic modalities, as well as novel "druggable" biomarkers for overcoming resistance to such treatments. This approach can be customized for any tumor types when appropriate genetic mouse models are available, and for testing of experimental targeted therapies[1,46]. Thus the applications of an integrated approach to the field of human cancer therapy are clearly significant, and potentially transformative.

URLs

ClinicalTrial.gov: http://www.clinicaltrials.gov

Taylor *et al.*, 2010: http://www.cbioportal.org/public-portal/index.do?cancer_study_id=mskcc_prad

Grasso *et al.*, 2012: http://www.ncbi.nlm.nih.gov/geo/query/acc.cgi?acc=GSE35988

Tomlins et al., 2007: http://www.ncbi.nlm.nih.gov/geo/query/acc.cgi?acc=GSE6099

NIH-PA Author Manuscript

NIH-PA Author Manuscript

NIH-PA Author Manuscript

Liu et al., 2009: http://www.ncbi.nlm.nih.gov/geo/query/acc.cgi?acc=GSE14996

Bioconductor *simpleaffy* package: http://www.bioconductor.org/

METHODS

Pten, p53 and *Lrf* mouse models

Previously generated $Pten^{flox/flox}$, $p53^{flox/flox}$ and $Lrf^{flox/flox}$ mice[5,13,47] were crossed with the *Probasin-Cre* mice[48] for the deletion of *Pten, p53* and *Lrf* specifically in the prostate epithelium. The pathological index (PI) we used was as follows: 0 (normal tissue), 1 (glands with a monolayer of epithelial cells with evident cellular neoplastic features), 2 (HG-PIN characterized by glands with more than 50% of cell-free lumen) to 3 (HG-PIN characterized by glands with less than 50% of cell-free lumen). Number of animals per genotype per experiment was estimated accordingly to the error variance. Mice were randomized and all the mouse work performed blindly to the genotype of the mice and in accordance with our IACUC approved protocol. For genotyping, tail DNA was subjected to PCR following the protocols previously described[5,13,47].

Western blot, immunohistochemistry and proliferation analysis on human and mouse prostate tissue

Cell lysates were prepared with RIPA buffer [1 X PBS, 1% Nonidet P40, 0.5% sodium deoxycholate, 0.1% SDS and protease inhibitor cocktail (Roche)] and cleaned by centrifugation. The following antibodies were used for Western blot analysis: mouse anti-cleaved Parp D214 (mouse specific), rabbit anti-Parp 46D11, rabbit anti-cleaved Caspase 3 (Asp175), rabbit anti-Gapdh 14C10, rabbit anti-XIAP 3B6 (Cell signaling), rabbit anti-AR PG-21 (Millipore), rabbit anti-Xaf1 SAB2900401 (Sigma), IMG-379 (Imgenex), goat anti-Probasin sc17126 (Santa Cruz). For immunohistochemistry, prostate tissues were fixed in 10% neutral-buffered formalin (Sigma) overnight, subsequently washed once with PBS, transferred into 50% ethanol and stored in 70% ethanol. Prostate lobes were embedded in paraffin, sectioned and stained with hematoxylin and eosin (H&E) in accordance with standard procedures. Sections were stained with the following antibodies: rabbit anti-Ki-67 (Novacastra), rabbit anti-AR (Millipore), rabbit anti-Xaf1 (Sigma), rabbit anti cleaved Caspase3 (Cell Signaling). Proliferative cells were identified by positive Ki-67 staining. A total of 5000 cells were counted from 50 different fields for each section for each lobe. The analysis was repeated on three different mice for each genotype.

MRI analysis

Mouse prostate images were acquired on an ASPECT Model M2 1T tabletop MRI scanner (ASPECT Magnet Technologies Ltd., Netanya, Israel). The M2 is a permanent magnet with zero magnetic fringe field. All mice were placed in the supplied 35mm mouse RF coil, calibrated to a RF frequency of between 43-45 MHz which is used for both transmission and reception. Prior to acquisition, mice were anesthetized with a mixture of isoflurane and oxygen via an external vaporizer at a percentage of 2.0 and 1.5%, respectively. Percentages were adjusted as needed during MR acquisition, as respiration was monitored using a small animal physiological monitoring system (BIOPAC Systems, Inc., Aero Camino Goleta, California). Scout images were acquired using a GRE steady state sequence to acquire images in all three orthogonal planes/orientations. For prostate imaging, mice were positioned in the center of the magnet with bladder used as the anatomical reference for the center point. Axial T2 weighted SE images were first acquired with the following parameters: FOV 40 × 40 mm, 1/0 mm thickness/gap, TR/TE of 4600/40 ms, 256 × 256 matrix, 2 NEX, and a dwell time of 30 μs. Subsequent to the T2 weighted scan, a T1 SE sequence was also acquired by simply changing the TR/TE values to 625/10 ms and

NIH-PA Author Manuscript

NIH-PA Author Manuscript

NIH-PA Author Manuscript

decreasing the dwell to 16μs. The NRG Console GUI performs online reconstruction which then allows data to be converted into DICOM files and archived for export into any image analysis software. Tumor volume quantification was performed as previously described[49].

Quantitative RT-PCR

Total RNA was prepared from mice frozen tissues using the Trizol method (Invitrogen). cDNA was obtained with iScriptTM cDNA Synthesis Kit (Bio-Rad). Triplicate samples for quantitative PCR were run in the Lightcycler 480 (Roche) using the SYBR Green I Master (Roche). Each value was adjusted by using Gapdh levels as reference (see Supplementary Table 4 for primer sequences).

Human mRNA profiling and aCGH analysis

CGH array data for 37 metastatic samples, yet pre-processed with RAE algorithm, were downloaded by GEO database (see URLs)[11]. CGH array data for 50 metastatic samples, pre-processed with RAE algorithm, were downloaded from GEO database (see URLs)[20]. Data for 13 EPI and 20 Metastatic patient samples analyzed on a spotted cDNA platform were obtained from GEO database (see URLs)[22]. 58 metastatic samples data were downloaded from GEO database and analyzed by Affymetrix Genome-Wide human single nucleotide polymorphism Array 6.0 (see URLs)[19]. MAS5 algorithm, as implemented in Bioconductor *simpleaffy* package (see URLs), was used to normalize raw data and Affymetrix annotation na31 to annotate probe-set ID to the corresponding Entrez Gene ID. Differential expression and statistical significance have been evaluated by Bioconductor *limma* package (see URLs). P-value lower than 0.05 were considered significant.

Patient samples

This study was performed after approval of the Institutional Review Board of the Dana-Farber Cancer Institute and Brigham and Women's Hospital, Boston, MA. Archival paraffin-embedded tissue blocks of prostate cancer from patients were retrieved from the Departments of Pathology from Beth Israel Deaconess Medical Center, Boston, and from the University of Ancona, Italy.

Tissue microarray construction, immunohistochemistry and image analysis

Among men in the study cohort, we obtained archival formalin-fixed, paraffin-embedded radical prostatectomy samples (n=87; all study subjects). The study pathologists (R.L., M.L.) reviewed H&E slides of each FFPE tissue block to select areas of tumor and benign tissue for construction of a tissue microarray (TMA). The TMA was constructed by taking three 0.6-mm cores of tumor tissue and two 0.6-mm cores of benign tissue per case from a formalin-fixed, primary tumor nodule and transferring each core to a recipient block. The tumor and benign specimens from all 87 cases were included on two different TMAs. We characterized the expression profile of PTEN, and LRF in tumors included on the TMAs by immunohistochemical evaluation of protein expression for each, using a BioGenex i6000 automated staining platform (BioGenex Laboratories Inc., Fremont CA). TMA sections were cut at 4μm, and subsequently deparaffinized in xylene, followed by a graded alcohol rehydration. Antigen retrieval was performed by microwaving the tissue in citrate buffer (LRF), or EDTA buffer (PTEN) for 5 minutes. Antisera for PTEN (Cell Signaling Technologies, Beverly, MA) and LRF (Novus Biologicals, Littleton, CO) were then applied (PTEN: 1/200 overnight; LRF: 1/500 for 1 hour). Primary antibody detection was performed using a polymer-HRP detection kit (Biogenix) with visualization achieved using a commercially available chromogenic DAB kit (Vector Laboratories Inc., Burlingame, CA). Finally, sections were counterstained with hematoxylin, and dehydrated in a graded series of alcohols prior to the application of a coverslip. TMA slides stained with either PTEN or

NIH-PA Author Manuscript

NIH-PA Author Manuscript

NIH-PA Author Manuscript

LRF were scanned using the CRi Vectra 200-slide scanning platform (v1.4.1, CRi/Caliper, Hopkinton, MA) following a standard bright-field scanning protocol. For each tumor core represented on the TMA, the system acquired images at 20nm intervals and combined them into a stack file that represents one image. To detect both DAB and hematoxylin, a maximum likelihood method was used to extract each spectrum, which represents each element of the IHC profile. The analysis of each core image stack was performed using InForm (v1.3, CRi/Caliper). To do this, a training set comprising two classes of tissue was created: 'tumor' and 'other'. Representative areas for each class were marked on 16-20 images from the TMA. Using the hematoxylin and DAB spectra, InForm was trained to differentiate between the two classes. Within the training set, InForm's ability to correctly differentiate tumor from other was determined by a trained pathologist (R.T.L), and the process was repeated until further training of InForm correctly identified all tumor tissue. IHC images were then analyzed using InForm's 'object-based' algorithm. The multispectral imaging profile obtained with the Vectra scanner allows the software to segment the nucleus and cytoplasm using the unmixed spectra of the nuclear counterstain and the DAB immunohistochemical stain used for each biomarker. To quantify the nuclear staining for each biomarker, the following parameters were employed: auto scale and fill hole were enabled, and the area was set to 0.15. For percentage analyses, a nuclear threshold for each biomarker was set as follows: PTEN was 0.288; LRF was 0.08. For cytoplasmic staining, the following parameters were set: the inner distance to nuclei was 0, the outer distance to nuclei was 7, the minimum size (pixel) was 1, and the threshold was 0.56. For percentage analyses, a cytoplasmic threshold for each biomarker was set as follows: PTEN was 0.066, LRF was 0.056. For each core, the DAB intensity of each biomarker for each cell is the determined by InForm. With a threshold applied, InForm calculated the percentage of cells that were positive for each biomarker in the nucleus, in the cytoplasm, and in both compartments. TMA cores that were difficult to classify due to technical limitations (complications with tissue presentation or core loss) were removed from all analyses. For the current analysis, of the 87 cases represented on the two TMA, three were removed from the analysis due to insufficient representation on the TMA (core loss). For all data metrics obtained, tissue samples were reviewed by a trained pathologist (R.T. L. and M.L.) to ensure appropriate assignment of scores.

In vitro treatments

VCaP, LnCaP, LnCaP C4-2, 22Rv1, PC3, and DU145 human prostate cancer cells were purchased from the ATCC, cultured in DMEM or RPMI medium (as indicated by the ATCC) supplemented with 10% FBS and tested for mycoplasma contamination every month. For androgen deprivation and drug treatments, the regular medium plus 10% FBS was replaced with regular medium supplemented with 10% charcoal/dextran treated FBS (Hyclone) (Steroid Free Medium) and 10 μM dutasteride, and/or 10 μM MDV3100, and/or 5μM embelin for 2 or 4 days. For siRNA experiments, cells were transfected with XIAP siRNA (obtained from Dharmacon) and 72 hrs after transfection, the regular medium plus 10% FBS was replaced with regular medium supplemented with 10% charcoal/dextran treated FBS (Hyclone) (Steroid Free Medium). For western blotting, cells were lysed in Ripa buffer (50 mM Tris pH 8.0, 150 mM NaCl, 1% NP-40, 0.5% deoxycholic acid, and 0.1% SDS) supplemented with protease inhibitors (Complete; Roche), briefly sonicated, and resolved on SDS-PAGE gels. The proteins were transferred to nitrocellulose membranes and detected by chemiluminescence after incubation with antibodies against PARP (1:1000, Cell Signaling), XIAP (1:1000, Cell Signaling), AR (1:1000, Millipore), Actin (1:4000, Sigma), GAPDH (Cell Signaling), and LRF (13E9).

NIH-PA Author Manuscript

NIH-PA Author Manuscript

NIH-PA Author Manuscript

In vivo treatments

Chemical castration studies in mice were conducted with bicalutamide (Casodex) at a dose of 10 mg/kg by oral gavage, daily for 5 days a week for 4 weeks. Tumor-bearing mice were treated with a combination of bicalutamide (10 mg/kg) plus XIAP inhibitor embelin (60 mg/kg) in 0.1% carboxymethyl cellulose (CMC) (as vehicle) by oral gavage, daily for 5 days a week for 4 weeks. Triple treatment experiments were conducted with bicalutamide (10 mg/kg) plus XIAP inhibitor embelin (60 mg/kg) in 0.1% carboxymethyl cellulose (CMC) (as vehicle) by oral gavage, 3 days a week and bicalutamide (10 mg/kg) plus Srd5a1 inhibitor dutasteride (XY mg/kg) in 0.1% carboxymethyl cellulose (CMC) (as vehicle) by oral gavage, 2 days a week for 4 weeks. Mice were euthanized and tumors were dissected, weighed, and processed for histopathology and molecular analyses at the conclusion of these studies.

Statistical Analysis—Results are expressed as mean ± SD. Comparisons between groups were assessed using Student's *t*-Test analysis. $P \leq 0.05$ was considered significant.

Supplementary Material

Refer to Web version on PubMed Central for supplementary material.

Acknowledgments

We would like to thank current members of the Pandolfi lab for critical discussion and Thomas Garvey for insightful editing. We are grateful to the Preclinical Murine Pharmacogenetics Facility at BIDMC and Dana-Farber/Harvard Cancer Center for expert support in all the aspects related to the work in mice. Dana-Farber/Harvard Cancer Center is supported in part by an NCI Cancer Center Support Grant # NIH 5 P30 CA06516. We also thank Dr. Abate-Shen for kindly providing the Probasin antibody, and the Small Animal Imaging Facility at BIDMC for the MRI imaging work. Additionally, we are grateful to Giuseppe Fedele and Xiaoqiu Wu from Loda's lab and the Center for Molecular Oncologic Pathology Dana-Farber/Brigham and Women's for their technical support in the generation, staining and analysis of the TMA. U.A. has been supported by a fellowship from the Italian Association for Cancer Research (AIRC) under grant IG-9408. AL has been supported in part by a fellowship from the Istituto Toscano Tumori (ITT, Italy). This work has been supported through the MMHCC/NCI grant (RC2 CA147940-01) to P.P.P.

REFERENCES

1. Nardella C, Lunardi A, Patnaik A, Cantley LC, Pandolfi PP. The APL paradigm and the “co-clinical trial” project. Cancer Discov. 2011; 1:108–16. [PubMed: 22116793]
2. Catalona WJ. Management of cancer of the prostate. N Engl J Med. 1994; 331:996–1004. [PubMed: 7880240]
3. Molina A, Belldegrun A. Novel therapeutic strategies for castration resistant prostate cancer: inhibition of persistent androgen production and androgen receptor mediated signaling. J Urol. 2011; 185:787–94. [PubMed: 21239012]
4. Wang G. Lrf suppresses prostate cancer through repression of a Sox9-dependent pathway for cellular senescence bypass and tumor invasion. Nat Genet. 2013 in press.
5. Chen Z, et al. Crucial role of p53-dependent cellular senescence in suppression of Pten-deficient tumorigenesis. Nature. 2005; 436:725–30. [PubMed: 16079851]
6. Schlomm T, et al. Clinical significance of p53 alterations in surgically treated prostate cancers. Mod Pathol. 2008; 21:1371–8. [PubMed: 18552821]
7. Tepper CG, et al. Profiling of gene expression changes caused by p53 gain-of-function mutant alleles in prostate cancer cells. Prostate. 2005; 65:375–89. [PubMed: 16037992]
8. Markert EK, Mizuno H, Vazquez A, Levine AJ. Molecular classification of prostate cancer using curated expression signatures. Proc Natl Acad Sci U S A. 2011; 108:21276–81. [PubMed: 22123976]

NIH-PA Author Manuscript

NIH-PA Author Manuscript

NIH-PA Author Manuscript

9. Abou-Kheir WG, Hynes PG, Martin PL, Pierce R, Kelly K. Characterizing the contribution of stem/progenitor cells to tumorigenesis in the Pten-/-TP53-/- prostate cancer model. Stem Cells. 2010; 28:2129–40. [PubMed: 20936707]
10. Kumar A, et al. Exome sequencing identifies a spectrum of mutation frequencies in advanced and lethal prostate cancers. Proc Natl Acad Sci U S A. 2011; 108:17087–92. [PubMed: 21949389]
11. Taylor BS, et al. Integrative genomic profiling of human prostate cancer. Cancer Cell. 2010; 18:11–22. [PubMed: 20579941]
12. Pourmand G, et al. Role of PTEN gene in progression of prostate cancer. Urol J. 2007; 4:95–100. [PubMed: 17701929]
13. Trotman LC, et al. Pten dose dictates cancer progression in the prostate. PLoS Biol. 2003; 1:E59. [PubMed: 14691534]
14. Wang S, et al. Prostate-specific deletion of the murine Pten tumor suppressor gene leads to metastatic prostate cancer. Cancer Cell. 2003; 4:209–21. [PubMed: 14522255]
15. Carver BS, et al. Reciprocal feedback regulation of PI3K and androgen receptor signaling in PTEN-deficient prostate cancer. Cancer Cell. 2011; 19:575–86. [PubMed: 21575859]
16. Zhang W, et al. Inhibition of tumor growth progression by antiandrogens and mTOR inhibitor in a Pten-deficient mouse model of prostate cancer. Cancer Res. 2009; 69:7466–72. [PubMed: 19738074]
17. Kent EC, Hussain MH. The patient with hormone-refractory prostate cancer: determining who, when, and how to treat. Urology. 2003; 62(Suppl 1):134–40. [PubMed: 14747051]
18. Kent EC, Hussain MH. Neoadjuvant Therapy for Prostate Cancer: An Oncologist's Perspective. Rev Urol. 2003; 5(Suppl 3):S28–37. [PubMed: 16985947]
19. Liu W, et al. Copy number analysis indicates monoclonal origin of lethal metastatic prostate cancer. Nat Med. 2009; 15:559–65. [PubMed: 19363497]
20. Grasso CS, et al. The mutational landscape of lethal castration-resistant prostate cancer. Nature. 2012; 487:239–43. [PubMed: 22722839]
21. Lee SU, Maeda T. POK/ZBTB proteins: an emerging family of proteins that regulate lymphoid development and function. Immunol Rev. 2012; 247:107–19. [PubMed: 22500835]
22. Tomlins SA, et al. Integrative molecular concept modeling of prostate cancer progression. Nat Genet. 2007; 39:41–51. [PubMed: 17173048]
23. Baretton GB, Klenk U, Diebold J, Schmeller N, Lohrs U. Proliferation- and apoptosis-associated factors in advanced prostatic carcinomas before and after androgen deprivation therapy: prognostic significance of p21/WAF1/CIP1 expression. Br J Cancer. 1999; 80:546–55. [PubMed: 10408865]
24. Gelmann EP. Molecular biology of the androgen receptor. J Clin Oncol. 2002; 20:3001–15. [PubMed: 12089231]
25. Liston P, et al. Identification of XAF1 as an antagonist of XIAP anti-Caspase activity. Nat Cell Biol. 2001; 3:128–33. [PubMed: 11175744]
26. Huang J, et al. XAF1 as a prognostic biomarker and therapeutic target in pancreatic cancer. Cancer Sci. 2010; 101:559–67. [PubMed: 19922503]
27. Tu SP, et al. Restoration of XAF1 expression induces apoptosis and inhibits tumor growth in gastric cancer. Int J Cancer. 2009; 125:688–97. [PubMed: 19358264]
28. Jiang C, Yi XP, Shen H, Li YX. Targeting X-linked inhibitor of apoptosis protein inhibits pancreatic cancer cell growth through p-Akt depletion. World J Gastroenterol. 2012; 18:2956–65. [PubMed: 22736919]
29. Dai Y, et al. Adenovirus-mediated down-regulation of X-linked inhibitor of apoptosis protein inhibits colon cancer. Mol Cancer Ther. 2009; 8:2762–70. [PubMed: 19737940]
30. Qiao L, et al. Gene expression profile in colon cancer cells with respect to XIAP expression status. Int J Colorectal Dis. 2009; 24:245–60. [PubMed: 18704457]
31. Dubrez-Daloz L, Dupoux A, Cartier J. IAPs: more than just inhibitors of apoptosis proteins. Cell Cycle. 2008; 7:1036–46. [PubMed: 18414036]
32. Nikolovska-Coleska Z, et al. Discovery of embelin as a cell-permeable, small- molecular weight inhibitor of XIAP through structure-based computational screening of a traditional herbal

NIH-PA Author Manuscript

NIH-PA Author Manuscript

NIH-PA Author Manuscript

medicine three-dimensional structure database. J Med Chem. 2004; 47:2430–40. [PubMed: 15115387]

33. Zou B, et al. XIAP-associated factor 1 (XAF1), a novel target of p53, enhances p53-mediated apoptosis via post-translational modification. Mol Carcinog. 2012; 51:422–32. [PubMed: 21678496]
34. Yamaoka M, Hara T, Kusaka M. Overcoming persistent dependency on androgen signaling after progression to castration-resistant prostate cancer. Clin Cancer Res. 2010; 16:4319–24. [PubMed: 20647476]
35. Chang KH, et al. Dihydrotestosterone synthesis bypasses testosterone to drive castration-resistant prostate cancer. Proc Natl Acad Sci U S A. 2011; 108:13728–33. [PubMed: 21795608]
36. Luo JH, et al. Gene expression analysis of prostate cancers. Mol Carcinog. 2002; 33:25–35. [PubMed: 11807955]
37. Liu P, et al. Sex-determining region Y box 4 is a transforming oncogene in human prostate cancer cells. Cancer Res. 2006; 66:4011–9. [PubMed: 16618720]
38. LaTulippe E, et al. Comprehensive gene expression analysis of prostate cancer reveals distinct transcriptional programs associated with metastatic disease. Cancer Res. 2002; 62:4499–506. [PubMed: 12154061]
39. Stephenson AJ, et al. Integration of gene expression profiling and clinical variables to predict prostate carcinoma recurrence after radical prostatectomy. Cancer. 2005; 104:290–8. [PubMed: 15948174]
40. Dai Y, et al. Natural IAP inhibitor Embelin enhances therapeutic efficacy of ionizing radiation in prostate cancer. Am J Cancer Res. 2011; 1:128–43. [PubMed: 21804946]
41. Taplin ME, et al. Phase II study of androgen synthesis inhibition with ketoconazole, hydrocortisone, and dutasteride in asymptomatic castration- resistant prostate cancer. Clin Cancer Res. 2009; 15:7099–105. [PubMed: 19887483]
42. Sartor O, Gomella LG, Gagnier P, Melich K, Dann R. Dutasteride and bicalutamide in patients with hormone-refractory prostate cancer: the Therapy Assessed by Rising PSA (TARP) study rationale and design. Can J Urol. 2009; 16:4806–12. [PubMed: 19796455]
43. Sartor O, et al. Activity of dutasteride plus ketoconazole in castration-refractory prostate cancer after progression on ketoconazole alone. Clin Genitourin Cancer. 2009; 7:E90–2. [PubMed: 19815488]
44. Varambally S, et al. Integrative genomic and proteomic analysis of prostate cancer reveals signatures of metastatic progression. Cancer Cell. 2005; 8:393–406. [PubMed: 16286247]
45. Danquah M, Duke CB 3rd, Patil R, Miller DD, Mahato RI. Combination Therapy of Antiandrogen and XIAP Inhibitor for Treating Advanced Prostate Cancer. Pharm Res. 2012; 29:2079–91. [PubMed: 22451249]
46. Chen Z, et al. A murine lung cancer co-clinical trial identifies genetic modifiers of therapeutic response. Nature. 2012; 483:613–7. [PubMed: 22425996]
47. Maeda T, et al. LRF is an essential downstream target of GATA1 in erythroid development and regulates BIM-dependent apoptosis. Dev Cell. 2009; 17:527–40. [PubMed: 19853566]
48. Wu X, et al. Generation of a prostate epithelial cell-specific Cre transgenic mouse model for tissue-specific gene ablation. Mech Dev. 2001; 101:61–9. [PubMed: 11231059]
49. Nastiuk KL, et al. In vivo MRI volumetric measurement of prostate regression and growth in mice. BMC Urol. 2007; 7:12. [PubMed: 17650332]

NIH-PA Author Manuscript

NIH-PA Author Manuscript

NIH-PA Author Manuscript

Editorial Summary (PF)

Pier Paolo Pandolfi and colleagues report that compound loss of Pten with Lrf or Trp53 leads to de novo resistance to androgen deprivation therapy in prostate cancer. Integrative analysis of mouse and patient data in a co-clinical approach identified XIAP and SRD5A1 inhibitors as potential therapies for castration-resistant prostate cancer.

NIH-PA Author Manuscript

NIH-PA Author Manuscript

NIH-PA Author Manuscript

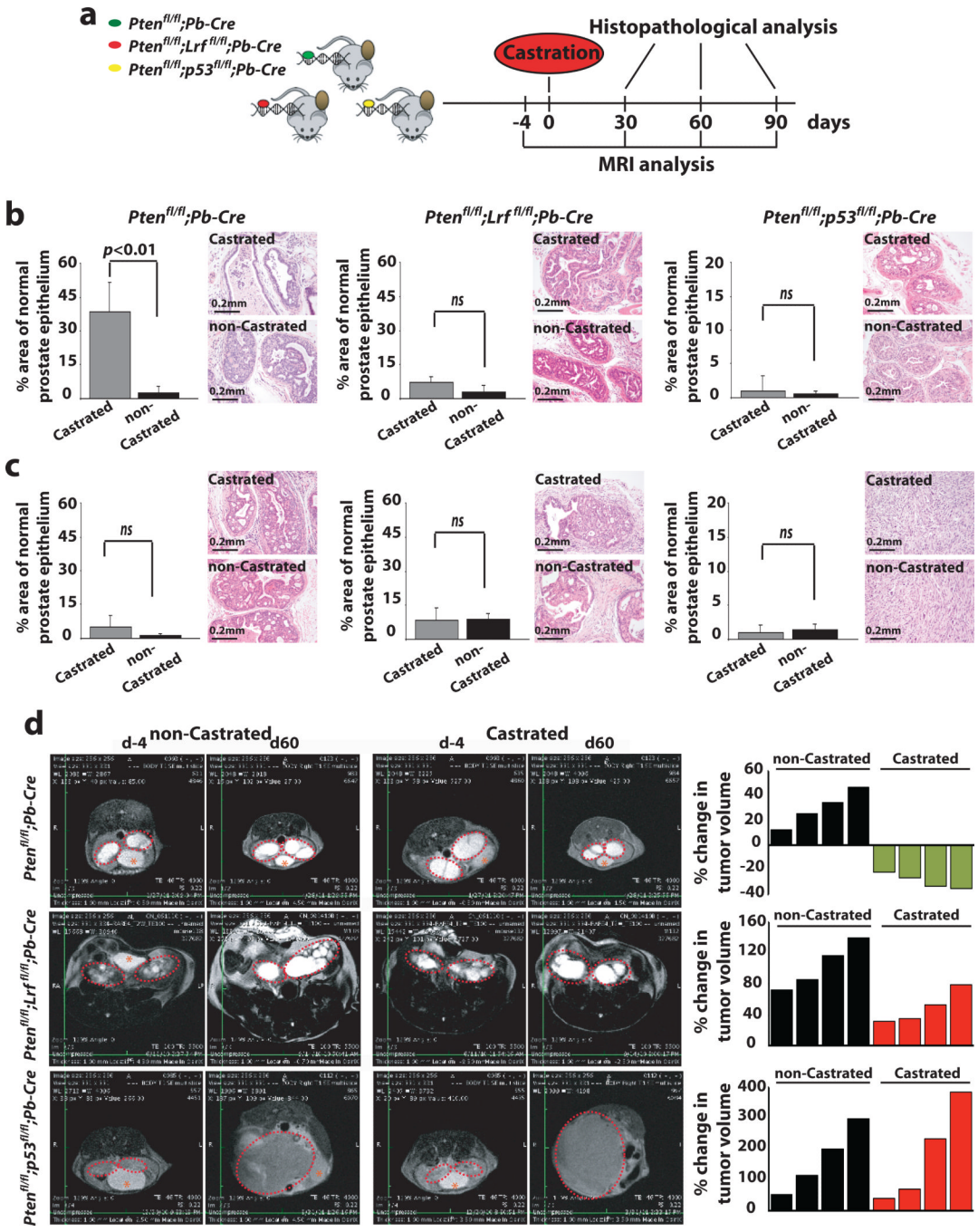

Figure 1. Prostate tumors characterized by distinct genetic alterations differentially respond to castration

(a) Timeline of analysis of Pten$^{flox/flox}$;Probasin(Pb)-Cre, Pten$^{flox/flox}$;Lrf$^{flox/flox}$;Probasin(Pb)-Cre, and *Pten$^{flox/flox}$;p53$^{flox/flox}$;Probasin(Pb)-Cre* noncastrated (n=15) and castrated (n=15) cohorts of mice. **(b-c)** Quantification of percentage area of normal epithelium in the prostate of *Pten$^{flox/flox}$;Probasin(Pb)-Cre* (left), *Pten$^{flox/flox}$;Lrf$^{flox/flox}$;Probasin(Pb)-Cre* (middle), and *Pten$^{flox/flox}$;p53$^{flox/flox}$;Probasin(Pb)-Cre* (right) castrated and non-castrated mice at 60 (**b**) and 90 (**c**) days post-castration. Representative images of H&E staining of DLP from castrated and non-castrated mice of the indicated genotypes are shown. **(d)** Representative MRI images of prostate cancers (Anterior

Lobe AP) in castrated and non-castrated mice of indicated genotype 4 days before and 60 days post-castration. Tumor volume (area outlined in red) was quantified as described in the experimental procedures. Asterisk represents the location of the bladder.

NIH-PA Author Manuscript
NIH-PA Author Manuscript
NIH-PA Author Manuscript

NIH-PA Author Manuscript

NIH-PA Author Manuscript

NIH-PA Author Manuscript

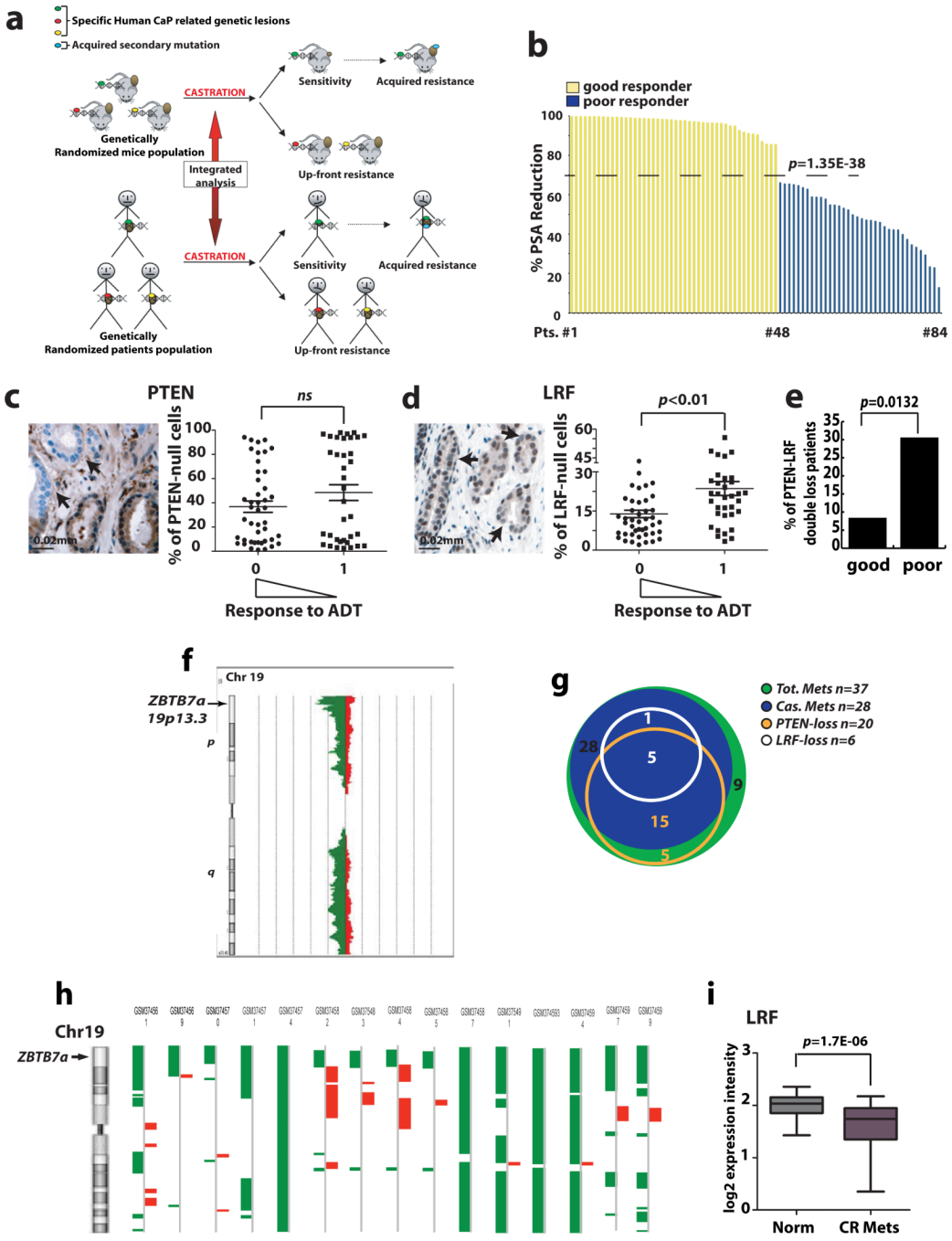

Figure 2. Analysis of human prostate cancer unveils the relevance of *LRF* loss in the response to androgen deprivation

(a) Cross-species integrated genetic screenings **(b)** Histogram showing the percentage of PSA-reduction following treatment used to stratify patients as good responders (yellow) or poor responders (blue) to ADT. Mean value of percentage of PSA reduction distribution is shown (dashed line). **(c-d)** PTEN and LRF IHC in human prostate cancer TMAs. The percentage of tumor cells with loss of PTEN and LRF were measured. Patients were considered good responders (0) or poor responders (1) to ADT according to the percentage of PSA reduction. Arrows highlight PTEN and LRF null cells. **(e)** Percentage of patients that experienced combined loss of PTEN and LRF in the category of good (8.7%) and poor

responders (30.5%). This distribution resulted statistically significant p=0.0132 in a Fisher test. **(f)** Schematic representation of the deletion of the *p* arm on chromosome 19 (green) in human CRPC. *ZBTB7a* genetic locus is indicated (arrow). **(g)** Diagram showing the distribution of *PTEN*-loss (orange) and *LRF*-loss (white) genetic alterations in castrated (blue) and noncastrated (green) metastasis. **(h)** CGH array data for 58 castration resistant prostate cancer metastatic samples shows genetic loss of the telomeric region of chromosome 19 containing the *Zbtb7a* locus. Data were processed by Partek Genomic Suite 6.4 Segmentation Algorithm (deletions are shown in green on the left side, amplification are showed in red on the right side). **(i)** Expression profile analysis of human castration resistant metastases shows statistically significant down-regulation of *LRF* expression.

NIH-PA Author Manuscript
NIH-PA Author Manuscript
NIH-PA Author Manuscript

NIH-PA Author Manuscript
NIH-PA Author Manuscript
NIH-PA Author Manuscript

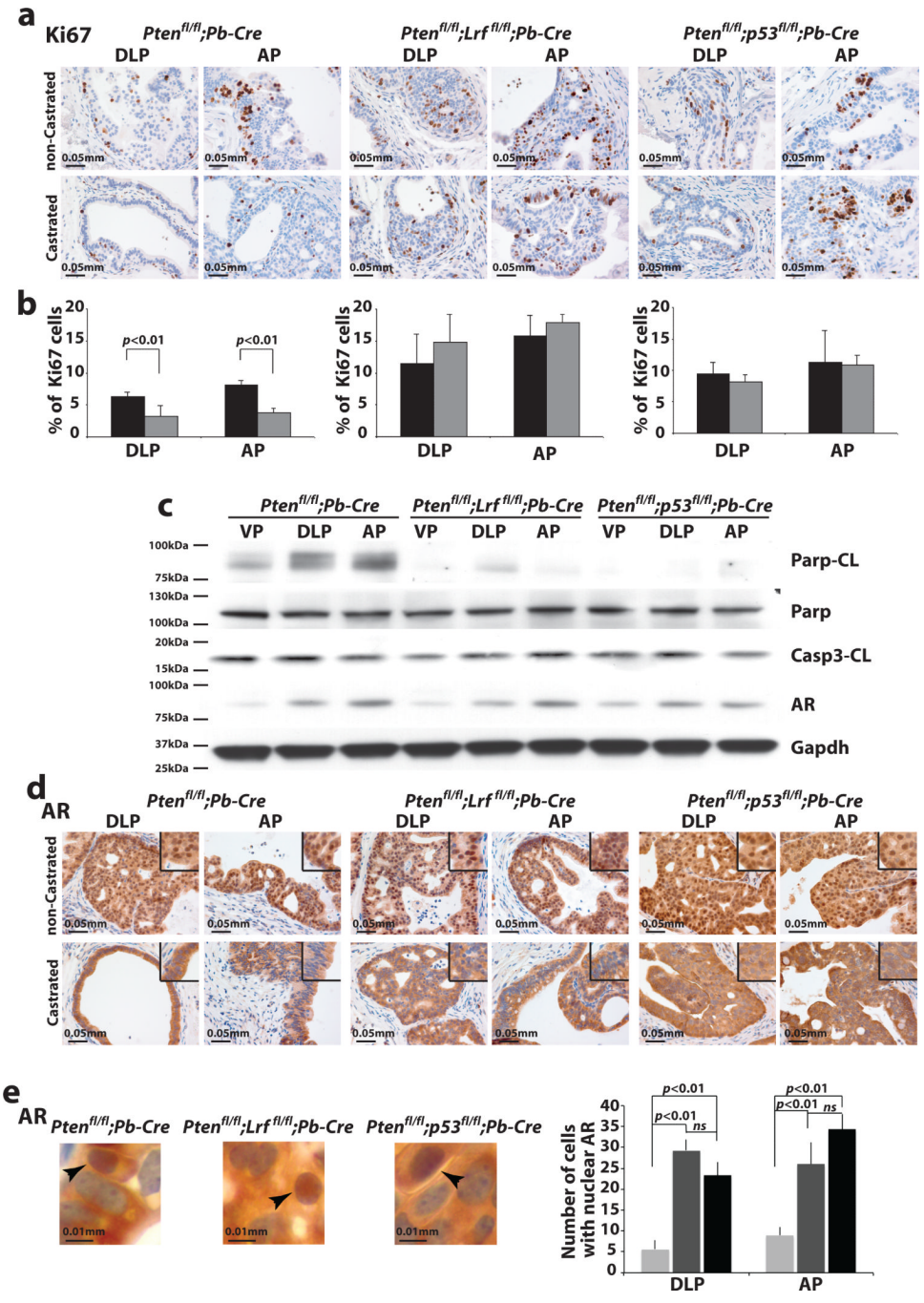

Figure 3. Differential responses to castration in different genetic backgrounds

(a-b) IHC staining of DLP and AP from castrated and non-castrated mice at 30 days post-castration. Upper panel: Ki-67 staining on prostate sections from castrated and noncastrated mice of indicated genotype. Lower panel: quantification of Ki-67 staining. Quantification has been performed as described in the methods. For each genotype, castrated (n=3, grey bar) and non-castrated (n=3, black bar) mice were analyzed. Percentage of Ki67 positive cells in DLP and AP prostate lobes was evaluated on a total of 15,000 cells per lobe. Data are presented as mean ± standard deviation. **(c)** Western blot analysis on VP, DLP and AP from castrated Pten$^{flox/flox}$;Probasin(Pb)-Cre, Pten$^{flox/flox}$;Lrf$^{flox/flox}$;Probasin(Pb)-Cre and

NIH-PA Author Manuscript

NIH-PA Author Manuscript

NIH-PA Author Manuscript

Pten$^{flox/flox}$;*p53*$^{flox/flox}$;*Probasin(Pb)-Cre* mice. Western blot analyses were performed on sample lysates collected from mice sacrificed 4 days after castration. **(d)** IHC staining of AR on DLP and AP from castrated and noncastrated mice sacrificed 30 days after castration. **(e)** Quantification of cells with nuclear AR localization in castrated *Pten*$^{flox/flox}$;*Probasin(Pb)-Cre* (light grey bar), *Pten*$^{flox/flox}$;*Lrf*$^{flox/flox}$;*Probasin(Pb)-Cre* (dark grey bar) and *Pten*$^{flox/flox}$;*p53*$^{flox/flox}$;*Probasin(Pb)-Cre* (black bar) prostate tumors. Number of cells with nuclear AR staining in DLP and AP prostate lobes was evaluated in n=3 castrated mice/genotype on a total of 2,500 cells for each prostate lobe. Data are presented as mean ± standard deviation.

NIH-PA Author Manuscript
NIH-PA Author Manuscript
NIH-PA Author Manuscript

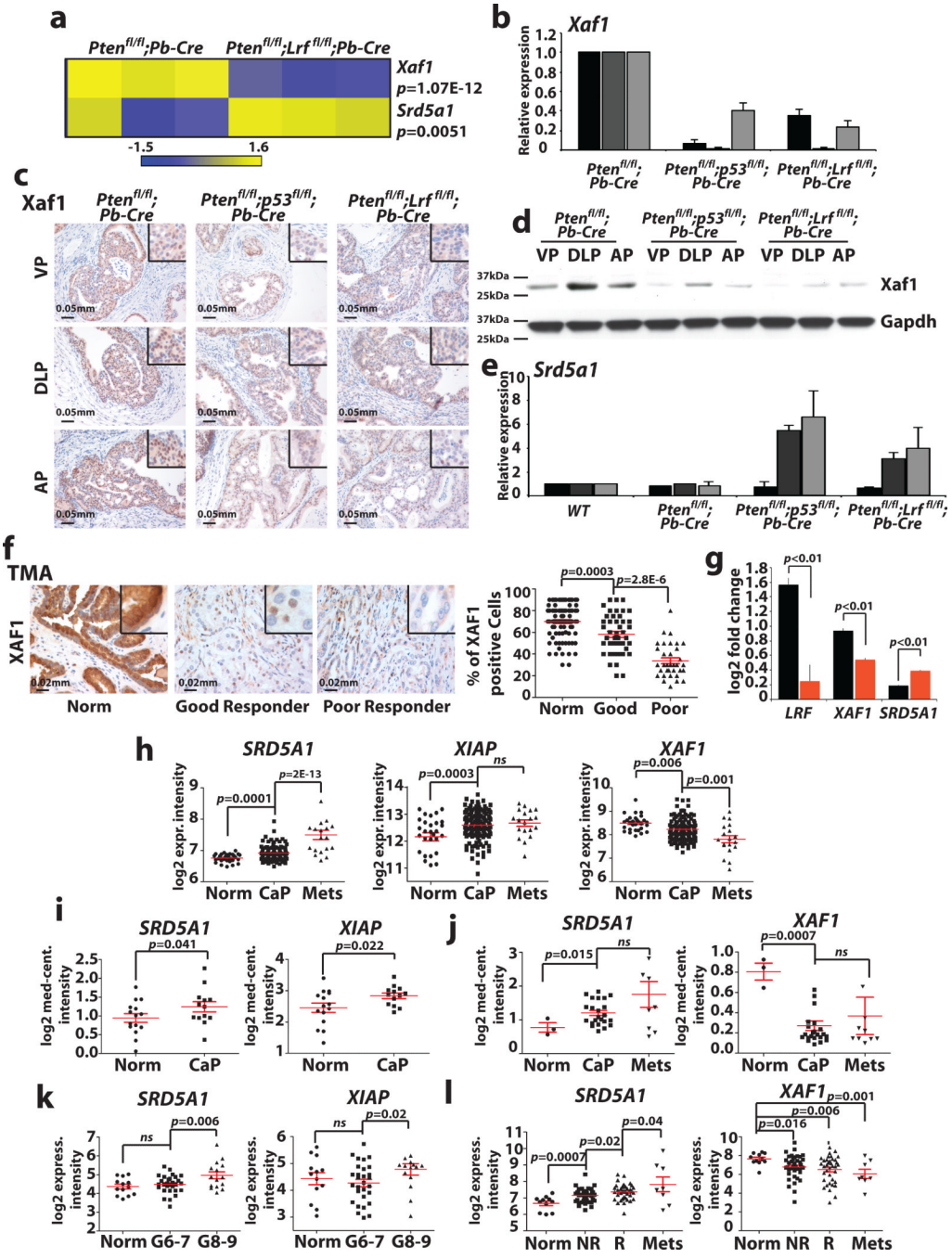

Figure 4. Deregulation of XAF1 and SRD5A1 levels dictates prostate cancer progression and castration resistance in mouse and human

(a) Analysis of the expression profiles of *Pten*$^{flox/flox}$*;Lrf*$^{flox/flox}$*;Probasin(Pb)-Cre* versus *Pten*$^{flox/flox}$*;Probasin(Pb)-Cre* prostates shows a significant down-regulation of *Xaf1* and a concomitant up-regulation of *Srd5a1*. **(b)** Quantitative RT-PCR of *Xaf1* in VP (n=3, black bars), DLP (n=3, dark grey bars) and AP (n=3, light grey bars) samples collected from Pten$^{flox/flox}$;Probasin(Pb)-Cre, Pten$^{flox/flox}$;Lrf$^{flox/flox}$;Probasin(Pb)-Cre, and *Pten*$^{flox/flox}$*;p53*$^{flox/flox}$*;Probasin(Pb)-Cre* mice. Data are presented as mean ± standard deviation. **(c)** IHC with anti-Xaf1 of the same samples in **b. (d)** Western blot analysis on the same samples in **b. (e)** Quantitative RT-PCR for *Srd5a1* in VP (n=3, black bars), DLP (n=3,

NIH-PA Author Manuscript

NIH-PA Author Manuscript

NIH-PA Author Manuscript

dark grey bars) and AP (n=3, light grey bars) samples collected from WT, Pten$^{flox/flox}$;Probasin(Pb)-Cre, Pten$^{flox/flox}$;Lrf$^{flox/flox}$;Probasin(Pb)-Cre and *Pten$^{flox/flox}$;p53$^{flox/flox}$;Probasin(Pb)-Cre* mouse prostates. Data are presented as mean ± standard deviation. **(f)** XAF1 staining and relative quantification in human prostate cancer TMA. **(g)** *LRF* and *XAF1* down regulation and *SRD5A1* induction in castration resistant prostate cancer xenografts (orange bars) versus castration sensitive (black bars). **(h-l)** *XAF1, XIAP*, and *SRD5A1* expression levels in primary and metastatic prostate cancer compared to normal prostatic epithelium.

NIH-PA Author Manuscript
NIH-PA Author Manuscript
NIH-PA Author Manuscript

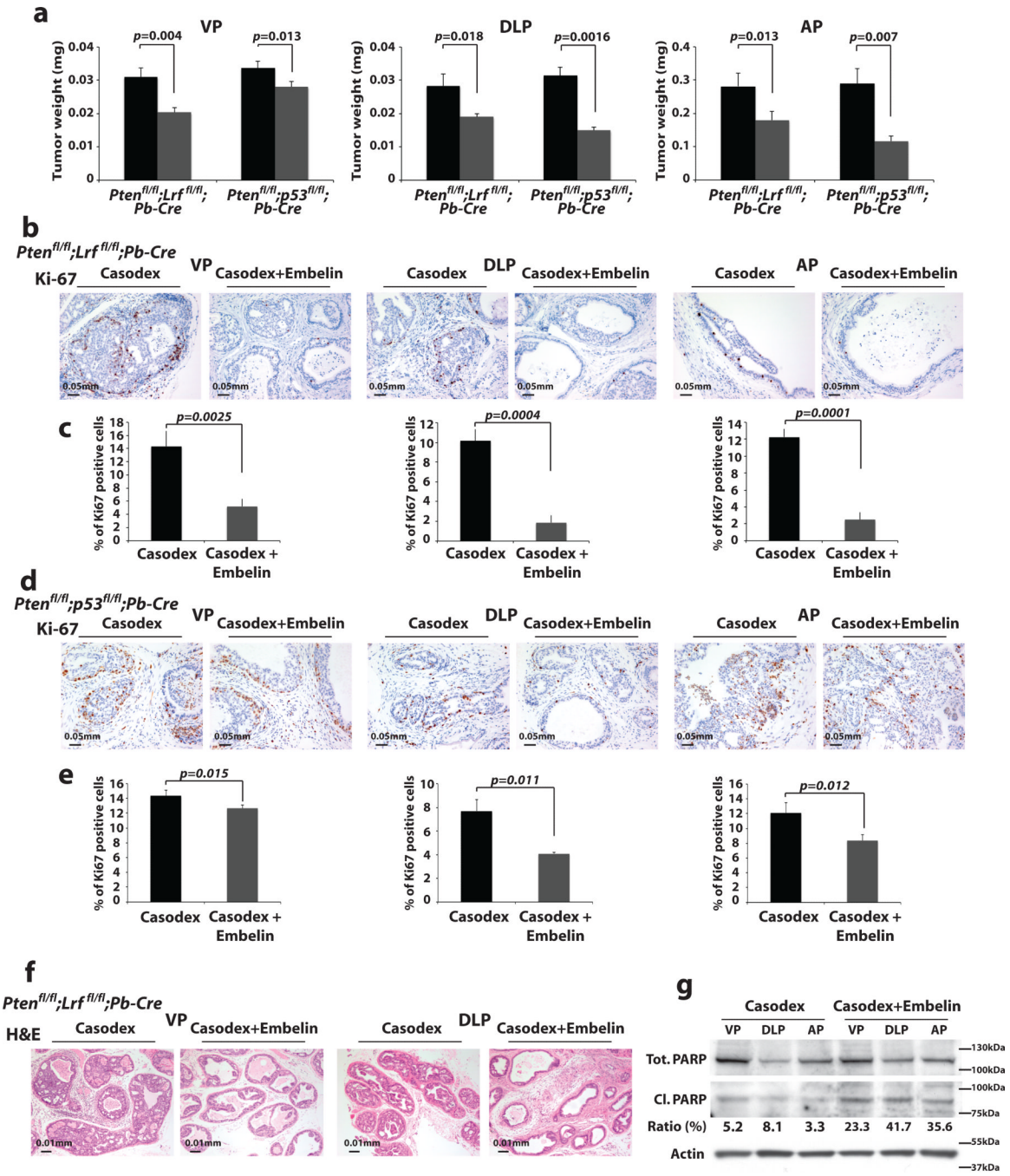

Figure 5. Synergistic effect of ADT and embelin, in mouse CRPC

(a) Weight of VP, DLP, and AP of *Pten*$^{flox/flox}$;*Lrf*$^{flox/flox}$;*Probasin(Pb)-Cre* and *Pten*$^{flox/flox}$;*p53*$^{flox/flox}$;*Probasin(Pb)-Cre* mice treated with bicalutamide (Casodex) (n=8) (black bars) or bicalutamide *plus* embelin (n=8) (grey bars) for 4 weeks. Data are presented as mean ± standard deviation. **(b-e)** Proliferation rate analysis as percentage of Ki67 positive cells in VP, DLP, and AP of the samples described in **a**. Data are presented as mean ± standard deviation. **(f-g)** H&E and apoptosis analysis through Western blot quantification of Parp cleavage versus total Parp in VP, DLP, and AP of the *Pten*$^{flox/flox}$;*Lrf*$^{flox/flox}$;*Probasin(Pb)-Cre* prostate cancers described in **a**.

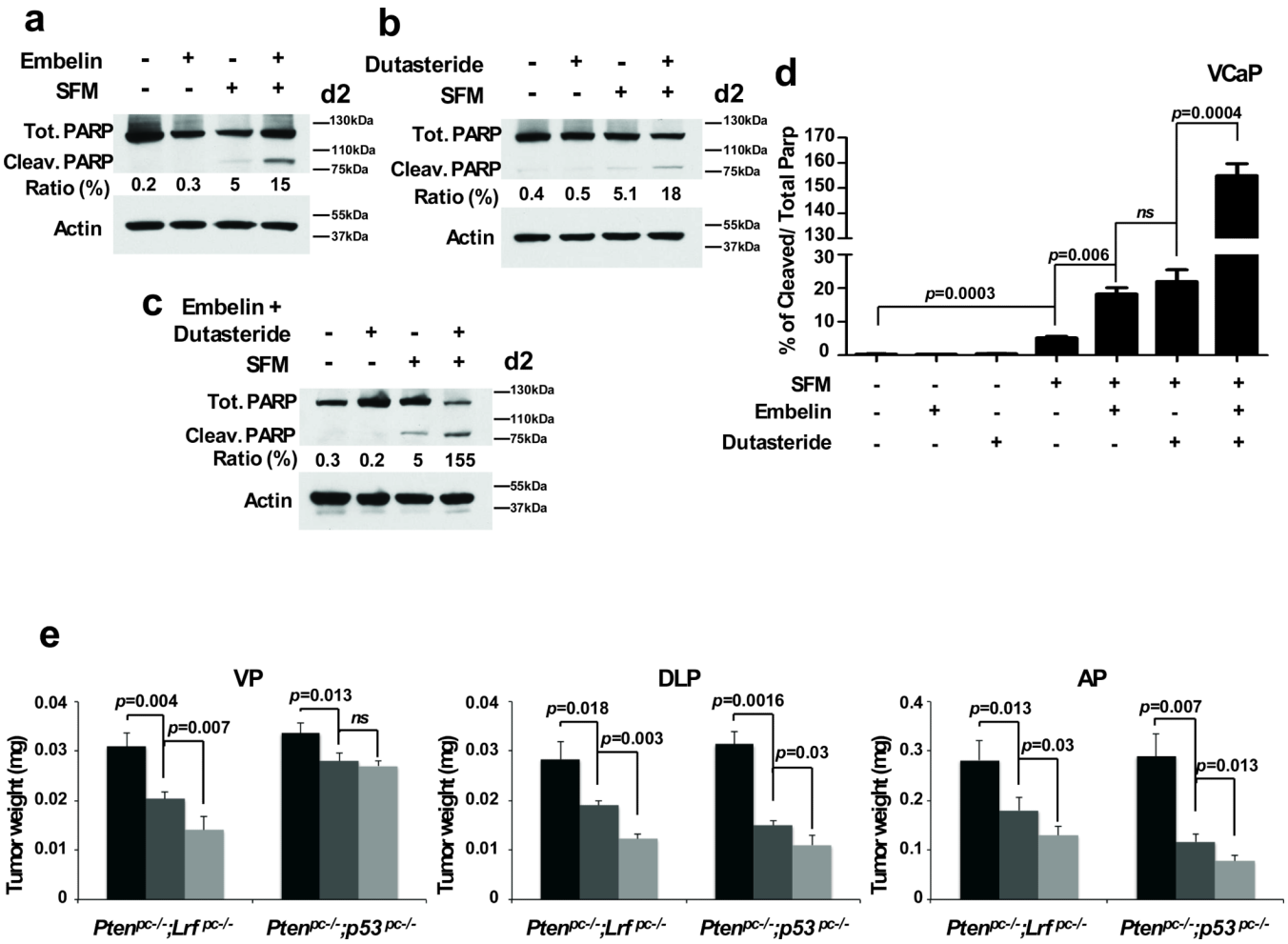

Figure 6. Genetic and molecular assessments in mice and patients dictate new experimental treatment to overcome CRPC

(a-d) Apoptosis analysis in human prostate cancer cell line (VCaP) treated with ADT, XIAP inhibitor (embelin), or SRD5A1 inhibitor (dutasteride), as single agent or in combination. Quantifications of PARP cleavage versus total PARP after 2 days of treatment are shown. **(e)** Weight of VP, DLP, and AP of castration resistant *Pten*$^{flox/flox}$;*Lrf*$^{flox/flox}$;*Probasin(Pb)-Cre* and *Pten*$^{flox/flox}$;*p53*$^{flox/flox}$;*Probasin(Pb)-Cre* mice treated with bicalutamide (Casodex) (n=4/genotype, black bars), bicalutamide plus embelin (n=4/genotype, dark grey bars), or bicalutamide plus embelin plus dutasteride (n=4/genotype, light grey bars) for 4 weeks. Data are presented as mean ± standard deviation.

NIH-PA Author Manuscript NIH-PA Author Manuscript NIH-PA Author Manuscript